# POSITION OF THE SOURCE OF DAYLIGHT HIGH-LATITUDE MAGNETIC PULSES IN THE MAGNETOSPHERE ACCORDING TO DMSP SATELLITE DATA

**©2025 Safargaleev V.V.**

*Pushkov Institute of Terrestrial Magnetism, Ionosphere and Radio Wave Propagation RAS, St. Petersburg Department, St. Petersburg, Russia*

*e-mail:Vladimir.safargaleev@pgia.ru*

Received March, 21 2024

Revised June, 27 2024

Accepted July, 25 2024

**Abstract.** Daytime high-latitude geophysical phenomena provide a ground-based observer with information about processes at the daytime magnetopause and/or in adjacent magnetospheric domains. It is assumed that these phenomena are initiated by changes in the parameters of the interplanetary medium and therefore can be used as a tool for studying the ways in which solar wind energy penetrates through the magnetopause. Such phenomena include magnetic impulses, which are an isolated train of damped oscillations of 2-3 bursts with a repetition period of 8-12 minutes. Using data from the Scandinavian network of magnetometers IMAGE, eight magnetic impulse events were studied for which DMSP satellites flew over the observation area during, shortly before and immediately after the pulse, crossing the boundaries of several domains. Based on ground-based and satellite data, it has been shown that the downward field-aligned current associated with the impulses is located away from the magnetopause. This means that the impulse cannot be considered as an ionospheric trace of a reconnected magnetic flux tube (flux transfer event, FTE) and/or as a traveling convection vortex (TCV). Using more statistics, it has been established that the pulse is preceded by noticeable changes in the *By* and *Bz* components of the IMF, while the contribution to the generation of the impulse from the pressure jump and solar wind speed, as well as the *Bx* component of the IMF, is not obvious. A possible scenario for the initiation of a magnetic pulse by IMF variations is discussed.

**Keywords:** *magnetic impulses, magnetospheric domains, equivalent ionospheric currents*

**DOI:** 10.31857/S00167940250107e8

# 1. INTRODUCTION

The key link in the formation of space weather is the input of energy and matter from the solar wind into the magnetosphere. A widely held view is that the penetration of energy and matter occurs primarily through the part of the dayside magnetopause, which "rests" with the footprints of its geomagnetic field lines on the high-latitude ionosphere near the noon meridian. This makes monitoring processes in the cusp and in the magnetospheric domains adjacent to the magnetopause—the low-latitude boundary layer ( *llbl* ), the boundary plasma sheet ( *bps* ), and the central plasma sheet ( *cps* )—an important element in studying the mechanisms of solar-terrestrial connections. The conjugation of these regions with the high-latitude ionosphere allows us to investigate the process of solar wind-magnetosphere interaction through a number of dayside phenomena observed from the Earth's surface. Based on DMSP satellite data ([Newell and Meng, 1992]), it can be asserted that during daytime hours and at different levels of geomagnetic activity, the magnetic stations of the IMAGE network located on Svalbard archipelago, near its southern coast, and on Bear Island "pass" under the projection of all the aforementioned magnetospheric formations.

Since the 1980s, magnetic impulse events ( *magnetic impulse events,* MIEs) have been considered as one of such ground-based phenomena. MIEs are isolated damping burst-like disturbances of the magnetic field, recorded by ground-based magnetometers at cusp latitudes (see, for example, [Lanzerotti el al., 1986]). At the initial stage of research, interest in this phenomenon was dictated by the fact that MIEs were interpreted as a ground signature of sporadic reconnection at the dayside magnetopause—so-called flux transfer events, FTE ([Goertz et al., 1985], [Lanzerotti el al., 1986] and references therein). As an alternative to reconnection, Sibeck [1992] proposed surface waves on the dayside magnetopause, generated as a result of the impact on the magnetosphere of a slow shock front at which plasma pressure rapidly changes ( *sudden impulses* , SI).

During the daytime hours in the European part of the eastern hemisphere, the magnetopause (the boundary between closed and open field lines) is statistically projected onto the northern part of Svalbard ([Newell and Meng, 1992]), where there is no dense observation network. Cases when the boundary descends so low that it falls, for example, into the field of view of the STARE radar over the northern coast of Norway ([Goertz et al., 1985]), are exotic. Magnetic impulses are rare but not exotic phenomena. Therefore, the hypothesis of Sibeck et al., 2003 seems more realistic, suggesting that magnetic impulses reflect in the ionosphere the development of the Kelvin-Helmholtz instability at the convection reversal boundary, which is considered the inner boundary *llbl* . It should be noted that the work of Clauer et al. [1997], referenced by Sibeck et al. [2003], was

devoted to the generation of pulsations with a period close to the period of burst sequences in a magnetic impulse. However, using two cases as examples, Yahnin et al. [1997] showed that the field-aligned current associated with MIEs is located deeper in the magnetosphere than the inner boundary of *llbl,* namely, inside the central plasma sheet, *cps.* Using different terminology to designate precipitation regions, Vorobiev [2004] concluded that traveling convection vortices (TCV), which are classified as "magnetic impulses," are generated in the polar part of the diffuse auroral zone, that is, equally deep in the magnetosphere. The question of which magnetospheric domains contain the source of MIEs remains debatable even today.

The probability of detecting magnetic impulses has a maximum in the 08-10 MLT interval (05-07 UT for high-latitude stations of the IMAGE network), and, as noted in the paper [Vorobyev et al., 1993], their appearance is not related to the southward turning of the *Bz* -component of the IMF. In most cases studied in this work, magnetic impulses were also observed at middle and low latitudes, which, according to the authors, indicates that deformation of the dayside magnetosphere is the cause of MIEs generation. The same conclusion was reached in [Yahnin et al., 1995] based on an analysis of a series of several events observed during one three-hour interval. Four cases where SI-initiated TCV phenomena could be associated with Kelvin-Helmholtz instability at the inner boundary of *llbl* are presented in [Sibeck et al., 2003].

One case of TCV caused by a sudden impulse was comprehensively investigated in a recent paper by Kim et al. [2017]. As noted above, TCVs are classified as magnetic impulses. The TCV and associated phenomena were observed by a large number of instruments both on the Earth's surface (magnetometer, radars, camera, and the scanning Doppler imager for complete sky coverage SCANDI) and on satellites (NOAA and DMSP). It was shown that the impulse is accompanied by enhanced precipitation, an increase in plasma temperature in the ionosphere, and a burst of magnetic activity in the hertz range. The authors also managed to identify its effect in the thermosphere. It is noted that the center of the convective vortex was located near the cusp. However, the interpretation of a bright spot amid other auroral forms as a result of precipitation from the cusp seems poorly substantiated.

The interpretation of magnetic impulses within the framework of SI does not agree with the results of Bering et al. [1990], according to which magnetic impulses are associated with strong changes in the IMF direction against the background of almost constant solar wind pressure. According to statistical studies by Konik et al. [1994], 50-70% of magnetic impulse events are associated with variations in the *By* - and *Bz* -components of the IMF, while only 15-30% of events followed changes in solar wind pressure.

Later, Moretto et al. [2004] noted that impulses appear more frequently during high-speed solar wind flow, but in general, impulse generation is determined by a wide range of conditions in the interplanetary medium.

It is known that in the transition region, as a result of the solar wind impinging on the magnetopause, a magnetic barrier is formed in which the magnetic field and concentration (plasma pressure) are interconnected. IMF variations generate plasma pressure variations which, similar to SC or SI, affect the magnetopause. As a result, the magnetopause becomes a source of secondary magnetosonic waves. Such qualitative reasoning is confirmed by the results of numerical modeling ([Lin et al., 1996]). The authors suggest considering these secondary waves as the cause of high-latitude magnetic impulses. A similar assumption was made in the work of [Vorobjev et al., 1999].

The peak of MIEs research occurred in the late 20th - early 21st centuries. However, the question of the nature of magnetic impulses (or TCV as one form of magnetic impulse) remains debatable even today. The aim of this work is to provide answers to the following two fundamentally important questions for understanding the nature of MIEs. The first question that arises when trying to connect magnetic impulse events with the processes of solar wind interaction with the magnetopause is in which magnetospheric domain their source is located. The answer to this will show how far from the magnetopause the source of the magnetic impulse is located. The second question is which variations of interplanetary medium parameters can be associated with the triggering of a magnetic impulse, and how these variations lead to the appearance of a source of magnetic impulses in regions of the magnetosphere distant from the magnetopause.

## 2. EQUIPMENT AND METHODOLOGY

The search for magnetic impulses was carried out using data from the IMAGE magnetometer network. The list of stations used for this purpose (as well as three low-latitude stations) with indication of code, geographic and geomagnetic coordinates is given in Table 1. The time interval of the search was 06:00-12:00 UT, which for the IMAGE stations listed in Table 1 corresponds to the interval of ~08:30-14:30 MLT. The above-mentioned interval of the most probable detection of MIEs lies within the search interval.

Table 1.

DMSP series satellites ( *Defense Meteorological Satellite Program* ) fly at an altitude of 840 km above the Earth's surface in near-polar orbits with an orbital period of 101 minutes, which gives a satellite velocity of approximately 7.5 km/s. At this speed, satellites fly over Svalbard for about 2 minutes. With pulse durations ranging from 5 to 25 minutes, there is a non-zero probability of

finding events when the satellite flies over the stations during a pulse, not just before or after it. The satellites are equipped, in particular, with a zenith-pointing particle detector (ten-channel spectrometer SSJ/4 ) that measures precipitating particles in the energy range from 30 eV to 30 keV with a time *resolution* of 1 s. To determine the boundaries of auroral invasions, an automatic algorithm proposed in [Newell et al., 1991] was used. The algorithm has been tested in several studies for prenoon precipitations (see, for example, [de la Beaujardiere et al., 1993]). In particular, good agreement is noted between the automatic and visual (using spectrograms) methods for determining the *bps/cps* boundary. We also note that according to statistical studies (see Fig. 2 in [Newell and Meng, 1992]), in the 9-12 MLT interval, the boundaries of magnetospheric domains are oriented predominantly along geomagnetic latitude. The magnetic pulse events analyzed in this work belong to this MLT interval.

DMSP data in the form of spectrograms with domain boundaries are obtained in *on-line* mode from the Johns Hopkins University website (Internet address http://sd-www.jhuapl.edu/Aurora/spectrogram/index.html ). The spectrograms show the coordinates of the sub-satellite point (see, for example, Fig. 2 *a* ), which, with the known satellite altitude, were used to calculate the projection of the satellite along the field line to the height of the *E* -layer of the ionosphere. For such heights, when projecting, it is sufficient to use only the IGRF model of the field line. In all figures below, the projection of the satellite trajectory is shown at a height of 100 km. At the beginning of the study, spectrograms were available up to 2015.

To clarify the position of the "base" of the longitudinal current, with the appearance of which we associate magnetic impulses (see Section 3 below), 1-D and 2-D distributions of ionospheric equivalent current intensity over the IMAGE network were calculated. The calculation was carried out in *on-line* mode on the network's website using the ECLAT program. The geomagnetic field value in the interval immediately before the beginning of the magnetic impulse was taken as the baseline. With this approach, the equivalent current distribution reflects the current disturbance whose magnetic effect is the magnetic impulse. To minimize the influence of disturbances not related to magnetic impulses, predominantly isolated events were analyzed, i.e., events with a relatively quiet geomagnetic pre-history. Even in these cases, due to the indistinct beginning of the magnetic impulse, the error in its determination was ±2 minutes. As a result, in further comparison of the impulse with variations in interplanetary medium parameters at the bow shock's nose, we could not obtain reliable statistics on such an important parameter as the delay time of the magnetosphere's response in the form of MIEs to IMF changes.

To analyze the situation in the interplanetary medium, we used data from the WIND and ACE satellites, which monitor the solar wind at a large distance from Earth, as well as from THEMIS satellites ( *Time History of Events and Macroscale Interactions during Substorms* ) during intervals when the satellites were outside the magnetosphere on the sunward side. When comparing with magnetic impulses, the propagation time of the disturbance from the satellite to the bow point on the shock front was taken into account. The coordinates of the satellites, as well as their distance to the shock front, were estimated using the *4D Orbit Viewer* ( https://sscweb.gsfc.nasa.gov/tipsod/ ).

In some cases, we had to resort to the OMNI service (https://cdaweb.gsfc.nasa.gov/index.html/ ), which recalculates the disturbance in the solar wind to the bow shock point in online mode. Keeping in mind the statistical studies by Ridley [2000], which showed that the uncertainty of recalculation by the OMNI service can be 8-25 minutes, preference was given to the analysis of direct satellite measurements.

Magnetic pulses are not an exceptional phenomenon. According to [Vorobyev et al., 1993], on average 0.5 pulses are detected per day. Experience working on the article gives a smaller figure: 2-4 events per month. Strict selection criteria (successful passes of DMSP satellites and quiet geomagnetic history of the pulse) led to the fact that for the period 2010-2014, only 8 cases were subjected to joint analysis with satellite measurements. Section 3 provides a detailed description of two cases. For the analysis of magnetic pulses in the context of the interplanetary medium situation, the database consisted of 22 cases. The results of this analysis are provided in section 4.

## 3. POSITION OF THE MAGNETIC PULSE SOURCE RELATIVE TO THE BOUNDARIES OF MAGNETOSPHERIC DOMAINS

This section provides a detailed analysis of two of the eight events for which data on the nature of precipitations over the observation area are available. The use of satellite data made it possible to approximately estimate the position of IMAGE stations and the presumed source of the pulse relative to the boundaries of magnetospheric domains.

### *3.1 Magnetic pulse on 05.03.2013. Source in the form of a current layer at the bps/cps boundary*

Fig. 1.

The pulse was recorded on the meridional chain of NAL-SOD stations of the IMAGE network around 06:09 UT on March 5, 2013. The change in pulse shape can be traced in Fig.1 *a* . On the three upper magnetograms of stations located on Svalbard, as well as at the HOP station south of Svalbard, the pulse begins with an increase in the $X$ -component of the geomagnetic field. We will refer to such deviations as a positive variation, meaning that the deviation is positive relative to the

field before the start of the pulse. The positive variation is caused by the strengthening of the equivalent ionospheric current in the eastern direction. On the magnetograms of stations located south of Svalbard (BJN, SOR, and SOD), the pulse begins as an excursion of the $X$ -component towards a decrease (negative variation), which corresponds to a strengthening of the western electrojet. For brevity, we will omit the characteristic "disturbed" in relation to the magnetic field, ionospheric and field-aligned currents, bearing in mind that we are talking about disturbed rather than absolute values of these parameters.

The distribution of ionospheric equivalent currents corresponding to the magnetic impulse is presented in Fig.1 *b* and c. (Color figures are available in the electronic version of the article). Recall that equivalent currents flow only in the ionosphere plane (presumably at an altitude of 100 km) and create the same magnetic field on the Earth's surface as the real system of ionospheric currents. The equivalent current system is not a real current system since it does not include field-aligned currents.

The diagram in Fig.1 *b* shows each vertical profile reflecting the current distribution along the meridian, averaged over a 10-second interval. Positive values correspond to eastward current. In the color figure in the electronic version of the article, the intensity of the eastward electrojet is represented by colors ranging from green to brown. At the moment of impulse onset at 06:09 UT, the transition region from westward to eastward electrojet was located between HOP and BJN stations (Fig.1 *b* ). In the color figure, the location where the current direction reverses from eastward to westward is clearly visible as a transition from red colors to blue through green. Gray horizontal lines indicate the latitudes of the stations.

On the 2D distribution map of the equivalent current, the ECLAT program identifies three foci of a clockwise vortex (Fig.1 *c* ). The direction and magnitude of currents are shown by vectors. Due to weak spatial resolution, the arrows at the ends of some vectors appear as thickenings. The results of calculating the 2-D current distribution in the area from the mainland (SOR station) to the pole should not be trusted unconditionally, as the magnetometer network is less dense at these latitudes than on the mainland. Nevertheless, the position of the vortex center is consistent with the location of the magnetic impulse polarity change on the magnetograms and diagram (Fig.1 *a* , *b* ). The vortex nature of ionospheric currents associated with magnetic impulses was noted at the initial stage of studying these phenomena (see, for example, the work of [Friis-Christensen et al., 1988]).

According to, for example, [Lyatsky and Maltsev, 1983], in the area where the ionospheric current changes direction from eastward to westward, the footprint of the field-aligned current (FAC) flowing into the ionosphere should be located current ( *field-aligned current* , FAC) . On 2D

maps of the equivalent ionospheric current, calculated using the ECLAT program, the trace of a localized field-aligned current flowing into the ionosphere is often associated with the center of a clockwise current vortex (for example, [Amm et al., 2002] and [Palin et al., 2016]), which is also the case in the example under consideration. Formally, the magnetic impulse is a product of approximately simultaneous intensification of eastward and westward jets. We propose to consider not the eastward and westward jets separately as the "source," but the field-aligned current that generates them together. Thus, determining the location of the impulse source in the magnetosphere is reduced to identifying precipitation regions (magnetospheric domains), within or at the boundary of which there is a current reversal area and/or the center of the current vortex.

Fig. 2.

Figure 2 *a* shows the spectrogram of electron and ion precipitations recorded by the DMSP F16 satellite during its passage over the observation area immediately after the magnetic impulse amplitude reached its maximum value (arrow in Fig.1 *a* ). During the passage, the satellite twice crossed the boundary between precipitations from *cps* and *bps* . Note that the satellite was taking measurements around 09:00 MLT, so according to the work by de la Beaujardiere et al.,1993 ], the automatic boundary determination algorithm can be trusted.

In Fig. 2 *b* the satellite trajectory is projected (along the geomagnetic field line) into the ionosphere at an altitude of 100 km. At this altitude, the ECLAT program calculates equivalent currents. The crossing points of *bps* are marked with gray crosses. The dashed lines passing through the crosses represent geomagnetic latitude. In Section 2, it was noted that in this MLT sector, the *bps* boundaries are oriented along geomagnetic latitude. Thus, the dashed lines show the *bps* boundaries beyond the satellite trajectory.

The square in Fig. 2 *b* marks the position of the vortex center located on the meridian 22°E, along which the diagram in Fig. 1 *b* was constructed. This and other centers are located along the equatorial boundary of *bps/cps* . It can be assumed that in this case, the field-aligned current had the form of a band and flowed at the boundary of *bps/cps* or near it. Thus, the source of the magnetic impulse was located inside the magnetosphere, away from the magnetopause and *llbl* , which does not allow linking the magnetic impulse with reconnection events at the magnetopause or with the Kelvin-Helmholtz instability in the convection reversal region ([Clauer et al., 1997]).

*3.2 Magnetic impulse on 21.04.2010. Satellite passage along the current sheet.*

The magnetic impulse was recorded at 06:45 UT (Fig. 3 *a* ). The analysis was conducted according to the same scheme as in the previous case. We include this event in the article for the following reason.

Fig. 3.

On the 2D current distribution map (Fig. 3 *c* ), the ECLAT program shows the presence of a fine structure in the vortex in the form of several foci. The westernmost focus is located approximately in the same place where, on the diagram (Fig. 3 *b* ), there is a reversal in the current direction. The vortex center also had a fine structure in the previous case (Fig. 1 *c* ). However, at that time, the satellite trajectory passed away from the center. In the present case, the satellite was flying directly over the series of foci (squares in Fig. 3 *d* ), while being in the precipitation region from *cps* Fig. 3 *g* ).

The lower panel of the spectrogram in Fig. 3 *g* shows that ion precipitations over the vortex centers had a sporadic character. As in the previous case, the vortex was rotating clockwise, indicating the presence of an inflowing (ions moving into the ionosphere) field-aligned current in its center. In light of this, we interpret the sporadic nature of ion precipitations as a sign of several filaments in the field-aligned current, generating a fine structure in the center of the vortex.

According to this scheme, we analyzed 8 events. In four cases, the source (more precisely, the center of the equivalent ionospheric current vortex) was located within the central plasma sheet ( *cps* ), in one case - within the boundary plasma sheet ( *bps* ), and in three cases - near the boundary between *bps* and *cps.* The analysis indicates that MIEs are neither flux transfer events at the magnetopause due to reconnection ( *FTE* events), nor Kelvin-Helmholtz instabilities developing at the inner boundary of *llbl* that generate propagating convection vortices in the ionosphere ( *TCV* events). In the next section, the appearance of magnetic impulses is considered in the context of changes in the interplanetary medium. In the Discussion section, based on the results of sections 3 and 4, a possible mechanism for magnetic impulse generation will be proposed.

## 4. MAGNETIC IMPULSES IN THE CONTEXT OF THE INTERPLANETARY MEDIUM SITUATION DEVELOPMENT

The statistics on this issue are more extensive, as the selection of events did not need to be limited to successful passes of the low-orbit DMSP satellites.

The results of the analysis are presented in Table 2. The first three columns indicate the number, date, and time of the magnetic impulse. The fourth column shows the amplitude of the solar wind pressure variation. Column 5 shows the amplitude of variation of the $X$ -component of the geomagnetic field at low-latitude observatories. The step-like variation at equatorial stations is

traditionally considered a sign of dayside magnetosphere compression during SI. Column 6 shows the relative changes in the x-component of the solar wind velocity. The + sign means that the velocity increased. Changes are classified as zero if the velocity changed by less than 5 km/s. Columns 7-9 show the values of the IMF components. The symbol 0.5/3.3 means that this component increased from +0.5 to +3.3 nT. The X symbol is used in cases where the component did not change or changed at the level of fluctuations (less than 0.5 nT).

For eight events of successful passage of DMSP satellites, column 10 indicates the name of the magnetospheric domain where, in our opinion, the source of the magnetic impulse was located. For example, the symbol *bps/cps* means that the source is located near the boundary between these domains. These events are placed at the beginning of Table 2.

Table 2.

In the Introduction, it was noted that the generation of magnetic impulses is determined not by a single factor, but by a wide range of conditions in the interplanetary medium ([Moretto et al., 2004]). We came to the same conclusion based on the results of our research. This is demonstrated in Fig. 4. Here, the magnetic impulse is considered in the context of measurements on the THB satellite. The satellite was on the Sun-Earth line at a relatively small (compared to the ACE and WIND satellites) distance from the shock wave front (~642,000 km, as provided by the *4D Orbit Viewer* service). With a solar wind speed of 340 km/s, the propagation time of the solar wind inhomogeneity from the satellite to the shock wave is 31 minutes. This time was taken into account when comparing satellite and ground data.

Fig. 4.

In Fig. 4, the variations of the IMF, velocity, and pressure of the solar wind on the THB and WIND satellites are given recalculated to the shock wave front . The gray area highlights the interval when a magnetic impulse was observed on the IMAGE network (see Fig. 3 *a* for this event). Approximately 4-5 minutes before the impulse began, the *Bx* -and *Bz* -components of the IMF rapidly change toward negative values. The *By* -component also changes rapidly in the same direction, but by a smaller amount. The IMF changes are accompanied by a rapid increase in the solar wind velocity by $\Delta\, Vx \sim 20$ km/s (6%).

Unlike the magnetic field and velocity, the solar wind pressure does not demonstrate a step-like change at the satellites either near the shock front or at a significant distance from it (solid and dashed lines in Fig. 4, respectively), characteristic of the phenomenon known in the literature as sudden impulse (SI). Nevertheless, the variation $X$ -component at the equatorial station AAE, $\Delta X$, in shape (but not in magnitude) resembles the magnetospheric response to SI (Fig. 4, bottom panel).

According to, for example, [Safargaleev et al., 2002], the typical magnitude of the geomagnetic response to SI at equatorial stations is $\Delta X \sim 40$ nT, which is 10 times larger. With the time *resolution* of AAE data of 1 minute, the moment of disturbance onset at AAE coincides within 1-2 minutes with the beginning of the magnetic impulse at high-latitude stations. If we assume that $\Delta X$ is somehow caused by changes in the IMF, we get an estimate of the propagation time of variation in the corresponding IMF component in the transition layer of ~ 4-5 minutes, which is consistent with the results of numerical modeling by Samsonov et al. [2006].

From Fig. 4, it follows that the variation of any of the presented parameters (except for the solar wind pressure) can be considered as a potential candidate for triggering the magnetic impulse.

Further research has shown that not all parameters of the interplanetary medium can be the cause of the magnetic impulse.

*4.1 The role of interplanetary medium parameters in triggering magnetic impulses*

Solar wind pressure impulse. Let's examine this parameter in more detail, as a number of authors believe that the sudden compression of the dayside magnetosphere leads to the generation of impulses ([Friis-Christensen et al., 1988]; [Sibeck, 1990]; [Vorobyev et al., 1993]; [Yahnin et al., 1995]; [Kim et al., 2017]). In [Yahnin et al., 1995], it is noted, in particular, that sometimes magnetic impulses are observed without global signs of SI. The authors attribute these signs to enhanced precipitation, changes in ionospheric conductivity, and bursts of geomagnetic activity in the ELF and ULF ranges. In the cited work, the presence/absence of global characteristics was not investigated. The case described in detail in [Kim et al., 2017] has signs of globality. The magnetospheric response to SI was multifaceted and manifested in precipitation and wave activity in the hertz range. The authors also found a response to SI at the thermosphere altitude.

For each event, we analyzed magnetograms from low-latitude stations Addis Ababa (AAE), Alibag (ABG), and Hermanus (HER). At these latitudes, the solar wind pressure impulse manifests as a step-like increase in the geomagnetic $X$ -component with a typical magnitude of ~40 nT (see, for example, [Safargaleev et al., 2002]). We consider this indicator as a necessary sign of SI globality. The appearance of the signs listed in [Yahnin et al., 1995] is largely determined by the state of the inner magnetosphere (in literature - the "preparedness" of the magnetosphere).

In the auroral zone, the response of the $X$ -component to SI also has a step-like form, reflecting the compression of the magnetic field, but pulsations in the *Pc5* range are additionally superimposed on the step (in literature - $P_{SI}5$ ). Despite the fact that periodicity in a similar range is also found in the magnetic impulse, no significant signs of SI or SC could be detected at equatorial stations. In

situations where an increase in the *X* -component was discernible against the background of fluctuations, this increase did not exceed 15 nT (see example in Fig. 5 *a* ).

Fig. 5.

As follows from Table 2 (column 4), minor but detectable to the naked eye step-like pressure changes sometimes occurred on the WIND satellite. However, some of them, when recalculated to the shock front, did not precede the impulse but were observed after its onset. Examples of such events are shown in the upper panels of Fig. 5 *a, b* .

The result does not agree with the results of a large number of earlier works (see, for example, [Yahnin et al., 1995] and references therein), where it was shown that SIs are the most likely triggers of MIEs. In this regard, we mention the work of Konik et al., [1994], which showed that the vast majority of magnetic impulses occur against the background of rapid changes in IMF components. The result does not unconditionally exclude SI as a trigger for impulses, since in the work Moretto et al., 1997 it was indicated that there are at least two different classes of TCV, differing in generation mechanisms.

Change in *Vx component* of solar wind velocity and *Bx* -component of IMF. Information about the nature of changes in these parameters is given in Table 2 (columns 6 and 7). It can be seen that in ~23% of cases *Vx* practically does not change (more precisely, changes at the level of fluctuations), in ~47% of cases *Vx* increases, and in ~30% of cases decreases. The argument for excluding this parameter from the list of possible candidates for triggering a magnetic impulse is not the diverse nature of the variation (increase or decrease in speed), but the delay relative to the onset of the impulse. In column 6, such events are marked with the symbol * and constitute ~23% of all events. This is also demonstrated by the example in Fig.5 *a, b* (second panel from the top).

*Bx* -component of the IMF changes more systematically - in 19 cases out of 22 *Bx* increases towards positive values. In 11 cases (50%), *Bx* passes through zero values. In the remaining cases, *Bx* remains either in the negative or positive range when changing. As with *Vx* , the argument to question the role of *Bx* in triggering the magnetic impulse is the inconsistency between the impulse start time and the moment when the *Bx* variation begins at the bow point of the shock wave front (events No. 4, 7, and 8 in Table 2, Fig. 5 *a, b* ).

We cannot explain the delay of *Vx* and *Bx* by inaccuracy in calculating the propagation time from the satellite to the shock wave front because the other two IMF components, whose variations begin before the magnetic impulse, were measured on the same satellite.

Variations of *By* - and *Bz* -components of the IMF as the most likely trigger for magnetic impulses. Above, solar wind pressure and velocity, as well as the *Bx* -component of the IMF, were

excluded from the list of candidates for triggering the magnetic impulse. The reason is that the variation of these parameters, which could be associated with the magnetic impulse, began after the impulse had already started. Information about the nature of changes in the two remaining parameters is given in Table 2 (columns 8 and 9).

In all considered cases, the *Bz* -component changed. The variations had different amplitudes and different signs, but unlike *Vx* and *Bx* , variations in the *Bz* -component began a few minutes before the start of the magnetic impulse (see examples in Fig. 5, third panel from the bottom). The *By* -component behaved in approximately the same way. Exceptions are two cases (No. 9 and 16 in Table 2) when the magnetic impulse began against the background of a smoothly decreasing By. Since there were distinct variations in the Bz component before the impulse, both of these components remain on the list of trigger candidates. This is illustrated by the example in Fig. 5 *a* (fourth panel from the top).

The result is consistent with the results of the statistical study by Konik et al. [1994], which showed that 50-70% of magnetic impulse events are associated with variations in *By* - and *Bz* - components of the IMF. Previously, Friis-Christensen et al., [1988] also linked the generation of magnetic impulses (in the form of TCV) with changes in these two components.

## 5. DISCUSSION

### *5.1 Ionospheric and field-aligned currents of the magnetic impulse. Generalization*

In all the studied situations, the magnetic impulse at high latitudes began as a positive deviation, while at lower latitudes the initial deviation was negative. That is, at high latitudes, the impulse was caused by an intensification of the eastward current, and below - the westward current. In the area where the equivalent ionospheric current changes direction from east to west, the footprint of the field-aligned current flowing into the ionosphere should be located current . On 2D maps of the equivalent ionospheric current, calculated using the ECLAT program, the trace of a localized field-aligned current flowing into the ionosphere is associated with the center of a clockwise twisted current vortex.

We assume that the magnetic impulse is a product of approximately simultaneous intensification of the eastern and western jets, caused by the strengthening or appearance of a localized inflowing field-aligned current. In all the events presented in the work, the disturbance of the field-aligned current occurred deep in the magnetosphere. The result may mean that the magnetic impulse is not a consequence of direct interaction of solar wind inhomogeneity with the magnetopause of the reconnection type or the development of the Kelvin-Helmholtz instability at the inner boundary of *llbl* .

*5.2 Magnetic impulse generation scenario*

Based on the generally accepted view that an Alfvén wave is a field-aligned current wave (see, for example, [Lyatsky and Maltsev, 1983]), we believe that the appearance of a field-aligned current, which is an indirect source of a magnetic impulse, is associated with the generation of an Alfvén wave. Below is a possible step-by-step scenario in which an Alfvén wave is generated in a local area inside the magnetosphere in response to changes in the IMF. The basis of the scenario consists of three theoretical results obtained earlier by other authors.

At the first stage, when entering the transition region between the shock wave and the magnetopause, IMF variations transform into plasma pressure variations. This can occur in the magnetic barrier region, where variations in the magnetic field and plasma concentration (plasma pressure) are interconnected. Such qualitative reasoning is confirmed by the results of numerical modeling ( Lin et al., 1996 ). We also note the work of Eastwood et al. [2008], where the phenomenon known in the literature as *hot flow anomalies* , HFA, is considered as a possible cause of pressure variations in the transition region in the absence of such in the solar wind. The authors propose to associate a short-term negative variation of the magnetic field on the ground-based network of observatories of the THEMIS project (Fig. 5 in the cited work) with these variations, calling it a magnetic impulse. The magnetic impulses considered in our study have a different form, and, unlike the work of Eastwood et al. [2008], the study is not a case study.

At the second stage, pressure variations, similar to SI, affect the magnetopause, as a result of which the magnetopause becomes a source of secondary waves of a magnetosonic type with a complex structure but small amplitude.

At the third stage, the shape of the magnetopause "comes into play" in the process. According to Leonovich and Kozlov [2020], the magnetopause, due to its shape, can act as a collecting lens, amplifying secondary waves or their effect in the "focus" located inside the dayside magnetosphere. Under the influence of the external environment, the shape of the magnetopause changes, and the position and dimensions of the focus change.

At the fourth stage, a complex wave (coupling of magnetosonic and Alfvén modes) propagates inside the magnetosphere. According to the theory of the magnetospheric Alfvén resonator, MHD disturbances from external regions transform into Alfvén oscillations during propagation deep into the magnetosphere. The transformation process is most effective at the geomagnetic latitude where the frequency of the external source coincides with the local frequency of the natural oscillations of the geomagnetic field line (see, for example, [Pilipenko, 2006 and references therein]). In the work by Leonovich and Mazur [1989], the transformation of a

magnetosonic wave into an Alfvén wave was studied in relation to SI events. The transformation occurs with both monochromatic and broadband forms of external excitation.

This theoretical result on the transformation of a magnetosonic wave into an Alfvén wave was used by the authors to explain pulsations $P_{SI}5$, which are the magnetosphere's response to SI. If the transformation region is in the "focus" of the magnetopause, the pumping effect will be noticeable.

In the model by Lühr et al. (1996) , the transformation of the fast compression wave mode into an Alfvén wave occurs at the density gradient, which is assumed to exist in the *llbl* . According to our study, the MIEs source is located deeper in the magnetosphere than the *llbl* .

The results of [Pilipenko et al., 2021] are in good agreement with our proposed scenario. Observations at conjugate points showed that TCV is excited by a magnetospheric current generator. The current generator mode corresponds to resonant oscillations in the magnetospheric Alfvén resonator. Such a resonant response to a magnetosonic pulse can indeed occur deep in the magnetosphere and is observed as MIEs/TCV.

It should be noted that the phenomena studied in this work are not pulses in the traditional sense of the word, but represent a train of damped oscillations. The bipolar nature of magnetic impulses was highlighted, in particular, in the work of Vorobyev et al. [1997]. The authors explained this feature by the movement of current vortices. Despite the fact that isolated events were selected for this study, they were not characterized by a distinct onset, which, combined with the relatively low temporal resolution of the magnetic data and the lack of a sufficient number of stations at the latitude where the vortex center was located, made it difficult to study the question of its movement. We believe that the pulsating form of the impulse could be caused by the bouncing of an Alfvén wave between conjugate ionospheres.

## 6. CONCLUSION

Magnetic impulses (MI or *magnetic impulse events* , MIEs) are a daytime high-latitude phenomenon in the form of an isolated train of damped pulsations in the $X$ -component of the geomagnetic field, consisting of 1−3 bursts with a repetition period of 8−12 minutes. We examined 22 cases of magnetic impulses whose current system consisted of oppositely directed ionospheric currents – eastward in the high-latitude part of the Scandinavian magnetometer network IMAGE and westward at stations located further south. On two-dimensional maps of the distribution of equivalent ionospheric currents, the current system had the form of a clockwise twisted vortex, in the polar part of which ionospheric currents flowed predominantly eastward, and in the southern part – westward.

For 8 cases, there were data on precipitating particles from DMSP satellites flying over the high-latitude part of the IMAGE network during, immediately before, or just after the magnetic pulse. Based on these data, the approximate position of the vortex center relative to the magnetospheric domain boundaries was determined. Considering the field-aligned current flowing into the vortex center as an indirect source of the magnetic pulse, it was shown that the source of the magnetic pulse is located either in the central plasma sheet, *cps* , or in the boundary plasma sheet, *bps* . This means that the previously proposed explanations of magnetic pulses by sporadic reconnection, surface waves on the magnetopause, or Kelvin-Helmholtz instability at the inner boundary of the low-latitude boundary layer, *llbl* , are not consistent with observations. The obtained result is consistent with the results of some case study format *case study* investigations (see, for example, [Yahnin et al., 1997]), thereby expanding the statistics on this issue.

All 22 cases of MIEs were analyzed in the context of the interplanetary medium situation. Based on the analysis results, sudden impulses (SI), solar wind velocity variations, and *Bx component* of the IMF were excluded from the list of possible candidates for triggering MIEs. The obtained result, excluding SI and indicating variations of *By* - and *Bz components* as the most likely trigger of MIEs, is consistent with the results of other studies (see, for example, Konik et al. [1994] ), thereby also expanding the statistics on this issue.

A step-by-step scenario for generating a magnetic impulse by the field-aligned current of an Alfvén wave is proposed. According to the scenario, variations in the IMF, passing through the region between the shock wave and the magnetopause, generate variations in plasma pressure. Pressure variations affect the magnetopause similar to SI phenomena, resulting in the magnetopause becoming a source of weak secondary mixed-type waves. The shape of the magnetopause resembles a converging lens, in the focus of which secondary waves are amplified. If a region of the magnetosphere appears in the focus where the energy of the mixed wave is "pumped" into the Alfvén mode (previously, the possibility of transforming a magnetosonic wave into an Alfvén wave was discussed in relation to the generation of pulsations $P_{SI}5$ ), the transformation will lead to the appearance of a field-aligned current. The vortex of the ionospheric equivalent current caused by the appearance of the field-aligned current will create a train of damping pulsations on the Earth's surface - a magnetic impulse.

ACKNOWLEDGMENTS

The author thanks Newell P.T. (Johns Hopkins University, APL, Laurel, Maryland, US) for preparing and posting information on the Internet about the position of auroral precipitation

boundaries based on observations from the DMSP satellite series. IMAGE network data are available on the website ( https://space.fmi.fi/MIRACLE ). Data from low-latitude stations AAE, ABG, and HER were taken from the global INTERMAGNET database ( https://imag-data.bgs.ac.uk/GIN_V1 ). The position of satellites was determined using the online procedure *SSC 4D Orbit Viewer* ( https://sscweb.gsfc.nasa.gov ). Geomagnetic latitude and local time were calculated using the online VITMO Model program ( https://omniweb.gsfc.nasa.gov/vitmo/cgm.html ).

FUNDING

This work was financially supported by the state assignment (state registration number 1021100714196-5).

REFERENCES

Vorobyev *V.G., Zverev V.L. Starkov G.V.* Geomagnetic impulses in the daytime high-latitude region: main morphological characteristics and connection with the dynamics of daytime auroras // Geomagnetism and Aeronomy. Vol. 33. 69-79. 1993.

Vorobyev *V.G., Zverev V.L.* Morphological features of traveling current vortices. // Geomagnetism and Aeronomy. Vol. 35. No. 5. P. 35-43. 1997

Lyatsky *V.B., Maltsev Yu.P.* Magnetosphere-ionosphere interaction. Moscow: Nauka, 192 p. 1983. - Pilipenko V.A. Resonance effects of ultra-low-frequency wave fields in near-Earth space // Abstract of dissertation of Doctor of Physical and Mathematical Sciences. Moscow: IPE RAS Publishing House, 33 p. 2006.

Amm *O., Engebretson M. J., Hughes T., Newitt L., Viljanen A., Watermann J.* A traveling convection vortex event study: Instantaneous ionospheric equivalent currents, estimation of fieldaligned currents, and the role of induced currents // J. Geophys. Res. V. 107. 1334. 2002. https://doi.org/10.1029/2002JA009472 .

Beaujardiere, *O. de la, Watermann J., Newell P., Rich F.* Relationship between Birkeland current regions, particle precipitation, and electric field // J. Geophys. Res. V. 98. P. 711-7720. 1993. https://doi.org/10.1029/92JA02005 .

Bering *III E. A., Lanzerotti L. J., Benbrook J. R., Lin Z.-M.* Solar wind properties observed during high-latitude impulsive perturbation events // Geophys. Res. Lett. V. 17. P. 579-582. 1990. https://doi.org/10.1029/GL017i005p00579 .

Clauer *C. R., Ridley A. J., Sitar R. J., Singer H. J., Rodger A. S., Friis-Christensen E., Papitashvili V. O.* Field line resonant pulsations associated with a strong dayside ionospheric shear convection flow reversal // J. Geophys. Res. V. 102. P. 4585 – 4596. 1997. https://doi.org/10.1029/96JA02929 .

- *Eastwood J. P., Sibeck D. G., Angelopoulos V., Phan T. D., Bale S. D., McFadden J. P., et al* . THEMIS observations of a hot flow anomaly: Solar wind, magnetosheath, and ground-based measurements // Geophys. Res. Lett. V. 35. N 17. 2008. https://doi.org/10.1029/2008GL033475 .

Friis-Christensen *E.; McHenry M. A., Clauer C. R., Vennerstrøm S.* Ionospheric traveling convection vortices observed near the polar cleft: A triggered response to sudden changes in the solar wind // Geophys. Res. Lett. V. 15. P. 253–256 . 1998. https://doi.org/10.1029/GL015i003p00253 .

Goertz *C. K., Nielsen E., Korth A., Glassmeier K. H., Haldoupis C., Hoeg P., Hayward D.* Observations of a possible ground signature of flux transfer events // J. Geophys. Res. V. 90. P. 4069–4078. 1985. https://doi.org/10.1029/JA090iA05p04069 .

Kim *H., Lessard M.R., Jones S.L. et al.* Simultaneous observations of traveling convection vortices: Ionosphere-thermosphere coupling // J. Geophys. Res. V. 122. P. 4943–4959. 2017. https://doi.org/10.1002/2017JA023904 .

Konik *R. M., Lanzerotti L. J., Wolfe A., Maclennan C. G., Venkatesan D.* Cusp latitude magnetic impulse events, 2, Interplanetary magnetic field and solar wind conditions // J. Geophys. Res. V. 99. P. 14831−14853. 1994. https://doi.org/10.1029/93JA03241 .

Lanzerotti *L. J., Lee L. C., Maclennan C. G., Wolfe A. and Medford L. V.* Possible evidence of flux transfer events in the polar ionosphere // Geophys. Res. Lett . 13. P. 1089−1092.1986. https://doi.org/10.1029/GL013i011p01089

Leonovich *A. S., Mazur V. A.* Resonance excitation of standing Alfven waves in an axisymmetric magnetosphere (nonstationary oscillations) // Planet. Space *Sci.* V. 37. P. 1109–1116. 1989. https://doi.org/10.1016/0032-0633(89)90082-2 .

Leonovich *A. S., Kozlov D. A.* Focusing of fast magnetosonic waves in the dayside magnetosphere // J. Geophys. Res. V. 125. e2020JA027925. 2020. https://doi.org/10.1029/2020JA027925 .

Lin *Y., Swift D. W., Lee L. C.* Simulation of pressure pulses in the bow shock and magnetosheath driven by variations in interplanetary magnetic field direction // J. Geophys. Res. V. 101. P. 2725−27269. 1996. https://doi.org/10.1029/96JA02733 .

Lühr *H., Lockwood M., Sandholt P. E., Hansen T. L., Moretto T.* Multi-instrument ground-based observations of a travelling convection vortices event // Ann. Geophys. V. 1. P. 162−181. 1996. https://doi.org/ 10.1007/s00585-996-0162-z

Moretto *T., Friis-Christensen E.; Lühr H., Zesta E* . Global perspective of ionospheric traveling convection vortices: Case studies of two Geospace Environmental Modeling events // J. Geophys. Res. V. 102. P. 11597–11610 . 1997. https://doi.org/10.1029/97JA00324

Moretto *T., Sibeck D., Watermann J.* Occurrence statistics of magnetic impulsive events // Annales Geophysicae. V. 22. P. 585−602. 2004. https://doi.org/10.5194/angeo-22-585-2004 .

Newell *P.T., Wing S., Meng C-I., Sigilitto V.* The auroral oval position, structure and intensity of precipitation from 1984 onward: an automated on-line base // J. Geophys. Res. V. 96. P. 5877−5882. 1991. https://doi.org/10.1029/90JA02450 .

Newell *P. T., Meng C.-I.* Mapping the dayside ionosphere to the magnetosphere according to particle precipitation characteristics // Geophys. Res. Lett. V.19. P. 609−612. 1992. https://doi.org/10.1029/92GL00404 .

Palin *L., Opgenoorth H. J., Årgen J., et al.* Modulation of the substorm current wedge by bursty bulk flows: 8 September 2002 – Revisited // J. Geophys. Res. V. 121. P. 4466–4482. 2016. https://doi.org/10.1002/2015JA022262 .

Pilipenko *V.A., Engebretson M.J., Hartinger M.D, Fedorov E.N., Coyle S.* , Electromagnetic fields of magnetospheric disturbances in the conjugate ionospheres: Current/voltage dichotomy / Cross-Scale Coupling and Energy Transfer in the Magnetosphere-Ionosphere-Thermosphere System, ed. by T. Nishimura, O. Verkhoglyadova, and Y. Deng, Elsevier B.V. Amsterdam. 357-440. 2021. https://doi.org/10.1016/B978-0-12-821366-7.00005-6 .

-*Ridley A. J.* Estimations of the uncertainty in timing the relationship between magnetospheric and solar wind processes // J. Atmos. Solar-Terr. Phys. V. 62. P. 757–771. 2000. https://doi.org/10.1016/S1364-6826(00)00057-2 .

-*Safargaleev V., Kangas J., Kozlovsky A., Vasilyev A.* Burst of ULF noise excited by sudden changes of solar wind dynamic pressure // Ann. Geophys. V.20. P. 1751–1761. 2002. https://doi.org/10.5194/angeo-20-1751-2002 .

-*Samsonov A. A., Nemeček Z., Šafránkova J.* Numerical MHD modeling of propagation of interplanetary shock through the magnetosheath // J. Geophys. Res. V. 111. A08210. 2006. https://doi.org/10.1029/2005JA011537 .

Sibeck *D. G.* A model for the transient magnetospheric response to sudden solar wind dynamic pressure variations // J. Geophys. Res. V. 95. P. 3755 – 3771.1990. https://doi.org/10.1029/JA095iA04p03755 .

- *Sibeck D. G.* Transient events in the outer magnetosphere: Boundary waves or flux transfer events? // J. Geophys. Res. V. 97. 4009–4026. 1992. https://doi.org/10.1029/91JA03017

- *Sibeck,D. G., Trivedi N. B., Zesta E., Decker R. B, Singer H. J., Szabo A., Tachihara H., Watermann J.* Pressure pulse interaction with the magnetosphere and ionosphere // J. Geophys. Res. V. 108. 1095. 2003. https://doi.org/10.1029/2002JA009675 .

Vorobjev *V.G., Yagodkina O.I. and Zverev V.L.* Morphological features of bipolar magnetic impulsive events and associated interplanetary medium signatures. // J. Geophys. Res. V. 104. P. 4595−4608. 1999. https://doi.org/10.1029/1998JA900042 .

- *Yahnin A., Titova E., Lubchich A., Bösinger T., Manninen J., Turunen T., Hansen T., Troshichev O., Kotikov A.* Dayside high latitude magnetic impulsive events: their characteristics and relationship to sudden impulses // J. Atmos. Solar-Terr. Phys. V. 57. P. 1569–1582. 1995. https://doi.org/10.1016/0021-9169(95)00090-O .

Yahnin *A. G., Vorobjev V. G., Bösinger T., Rasinkangas R., Sibeck D. G., Newell P. T.* On the source region of traveling convection vortices // Geophys. Res. Lett. V. 24. P. 237–240. 1997. https://doi.org/10.1029/96GL03969 .

**Table 1** . Coordinates of magnetic stations

| Code | Observatory | Geographic coordinates | | Geomagnetic latitude, ° N | MLT, h |
|---|---|---|---|---|---|
| | | latitude, ° N | longitude, ° E | | |
| NAL | Ny Ålesund | 78.92 | 11.95 | 75.25 | UT+2.7 |
| LYR | Longyerbyen | 78.20 | 15.82 | 75.12 | UT+2.8 |
| HOR | Hornsund | 77.00 | 15.60 | 74.13 | UT+2.6 |
| HOP | Hopen Island | 76.51 | 25.01 | 73.06 | UT+2.9 |
| BJN | Bear Island | 74.50 | 19.20 | 71.83 | UT+2.7 |
| SOR | Sørøya | 70.54 | 22.22 | 67.70 | UT+2.7 |
| SOD | Sodankylä | 67.37 | 26.63 | 63.92 | UT+2.3 |
| NUR | Nurmijärvi | 60.50 | 24.65 | 56.89 | UT+1.8 |
| ABG | Alibag | 18.64 | 72.87 | 10.69 | |
| AAE | Addis Ababa | 9.03 | 38.77 | 5.4 | |
| HER | Hermanus | -34.42 | 19.23 | 34.03 | |

**Table 2** . Magnetic impulses and interplanetary medium parameters

| No. | dd/mm/yyyy | UT | Δ *P* , nPa | ΔX, nT | ΔVx, % | IMF | | | domain |
|---|---|---|---|---|---|---|---|---|---|
| | | | | | | *Bx* | *By* | *Bz* | |
| 1 | 2 | 3 | 4 | 5 | 6 | 7 | 8 | 9 | 10 |
| 1 | 21/04/2010 | 06:46 | ~0 | 4 | +8* | 5/2 | -2.6/-4 | 0/-4 | *cps* |
| 2 | 24/04/2010 | 08:45 | ~0 | 1.5 | +8 | -4/1 | 0.5/4.5 | -1/1 | *cps* |
| 3 | 10/01/2011 | 08:16 | ~0 | ~1 | -3 | -2/2 | 0/-2 | -3/3 | *cps* |
| 4 | 20/01/2011 | 08:42 | 0.35 | 3.5 | +4* | -3/1* | 2/0 | -1/1.7 | *bps/cps* |
| 5 | 15/02/2011 | 06:54 | ~0 | ~7 | +9 | -5/1 | 3/1 | 2/6 | *bps/cps* |
| 6 | 04/06/2011 | 07:51 | 0.4 | ~5 | ~0 | 2/3 | 0.5/-2.5 | -3/1 | *cps* |
| 7 | 05/03/2013 | 06:09 | ~0 | 2 | +3 | 3/-1* | -0.5/-2 | 1/-1 | *bps/cps* |
| 8 | 18/10/2014 | 07:37 | ~2 | ~2 | -2* | 0/-2.5* | 4/1 | 2/0 | *bps* |
| 9 | 06/01/2010 | 06:07 | 0.25 | 13** | -5 | 0/2.5 | X | 4/-2 | |
| 10 | 29/01/2010 | 05:05 | 1.1 | 13 | ~0 | -1/2.5 | 2.2/4 | 3/0 | |
| 11 | 17/01/2011 | 08:38 | 0.5 | ~2 | +6* | -4.5/-3 | 0/2.5 | -1/0 | |
| 12 | 26/08/2011 | 06:31 | ~0 | ~1 | -7 | 0/4 | -4/0 | -1/1 | |
| 13 | 07/11/2011 | 06:07 | 0.8 | 0 | ~0 | 0/1 | 0/-3 | 1/3 | |
| 14 | 08/02/2012 | 06:05 | ~0 | ~1 | -3 | -3/1 | 0/-3 | 1.5/4 | |
| 15 | 29/02/2012 | 07:22 | 1.5 | ~8 | +3 | -5/1 | 2/4 | 2/-4 | |
| 16 | 16/02/2013 | 07:42 | 0.2 | 0 | ~0 | -2.5/-2 | X | 0/-2 | |

| | | | | | | | | | |
|---|---|---|---|---|---|---|---|---|---|
| 17 | 03/03/2013 | 08:37 | ~0 | 10 | +9* | 4.5/2.5 | 0/-4 | -2/1 | |
| 18 | 16/10/2013 | 08:45 | 0.4 | 3 | +3 | -3/-1.5 | -1.2 | -1.5/1 | |
| 19 | 18/10/2013 | 06:05 | ~0 | ~0 | +4 | -3.5/-2 | -1/3 | 1/0 | |
| 20 | 28/10/2013 | 09:11 | 0.4 | 10 | ~0 | 0.5/1.2 | -0/-4.7 | 4.5/0 | |
| 21 | 20/04/2014 | 07:28 | 0.5 | ~0 | -2 | -5/-2 | 1/0 | 1/4 | |
| 22 | 06/10/2014 | 06:33 | 2 | 2 | +2.5 | 3/4 | -3/0 | 0.5/2.5 | |

*Note:* Symbol * refers to a parameter whose variation onset does not match the beginning of the magnetic impulse. Symbol ** indicates pressure change in eV/cm $^3$

Figure captions

**Fig. 1** . ( *a* ) − Magnetic impulse on the IMAGE station chain (highlighted in gray). The moment of the F16 satellite passage is shown by an arrow. ( *b* ) − 1D distribution of the equivalent ionospheric current, showing the dynamics of eastward (+) and westward (-) currents of the magnetic impulse at the 22° E meridian. ( *c)* − Vortex character of the equivalent current distribution. Current direction is shown by arrows.

**Fig. 2.** ( *a* ) − Character of precipitations along the satellite trajectory with indication of magnetospheric domains three minutes after the pulse onset. ( *b* ) − Fragment of the F16 trajectory. The position of the *cps/bps* boundaries is shown by crosses. The precipitation region from *bps* is filled with gray. Dashed line – geomagnetic latitude (domain boundaries outside the trajectory). Square – vortex center at the 22°E meridian, along which the 1D distribution of equivalent current was calculated in Fig. 1 *b*

**Fig. 3.** ( *a* ) − Antiphase nature of magnetic field variations. The arrow shows the moment when the F17 satellite flew over the IMAGE network. ( *b* ) − Dynamics of eastward (+) and westward (-) currents of the magnetic pulse at the 22° E meridian. Thin vertical line – the time moment for which the equivalent current map was calculated. ( *c* ) − Vortex structure with multiple centers on the equivalent current map of the magnetic pulse. Current direction is shown by arrows. ( *d* ) − Character of precipitations over the observation area according to DMSP F17 data. ( *e* ) − Fragment of the F17 trajectory. Crosses – reference points for trajectory plotting. Squares – position of the vortex center.

**Fig. 4.** Variations of interplanetary medium parameters at the bow shock standoff point for the time interval including the magnetic pulse observation period (highlighted in gray, see also Fig. 3 *a* ).

From top to bottom: solar wind velocity and pressure, three components of IMF. Bottom panel – step-like increase of the *X* -component of the geomagnetic field at the equatorial station AAE.

**Fig. 5.** Three examples of magnetic pulses (intervals highlighted in gray) in the context of interplanetary medium parameter changes at the bow shock standoff point. From top to bottom: variations in solar wind pressure and velocity, IMF variations, magnetograms of IMAGE network stations demonstrating the antiphase nature of the magnetic pulse, variations of the geomagnetic field at equatorial stations.

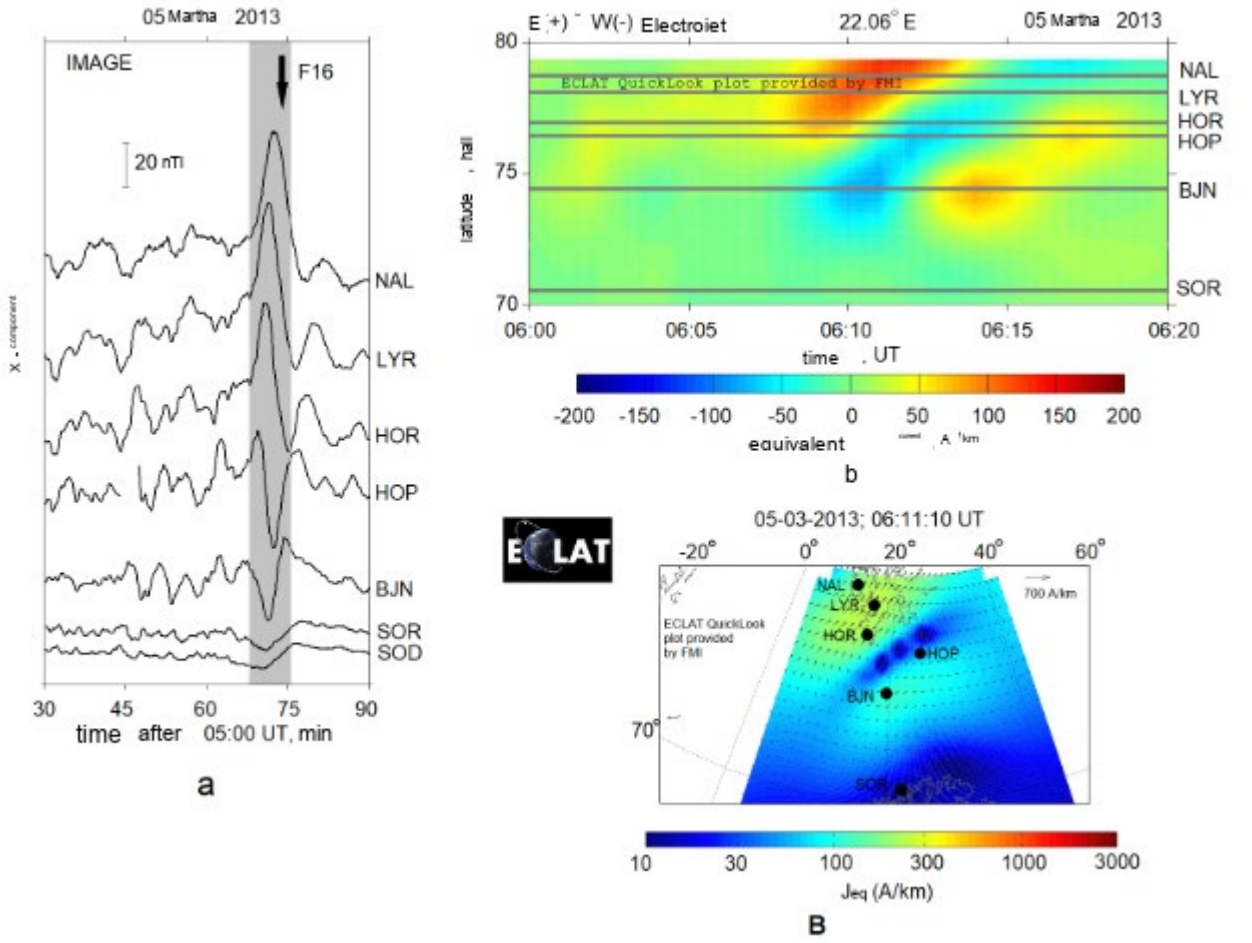


Fig. 1.

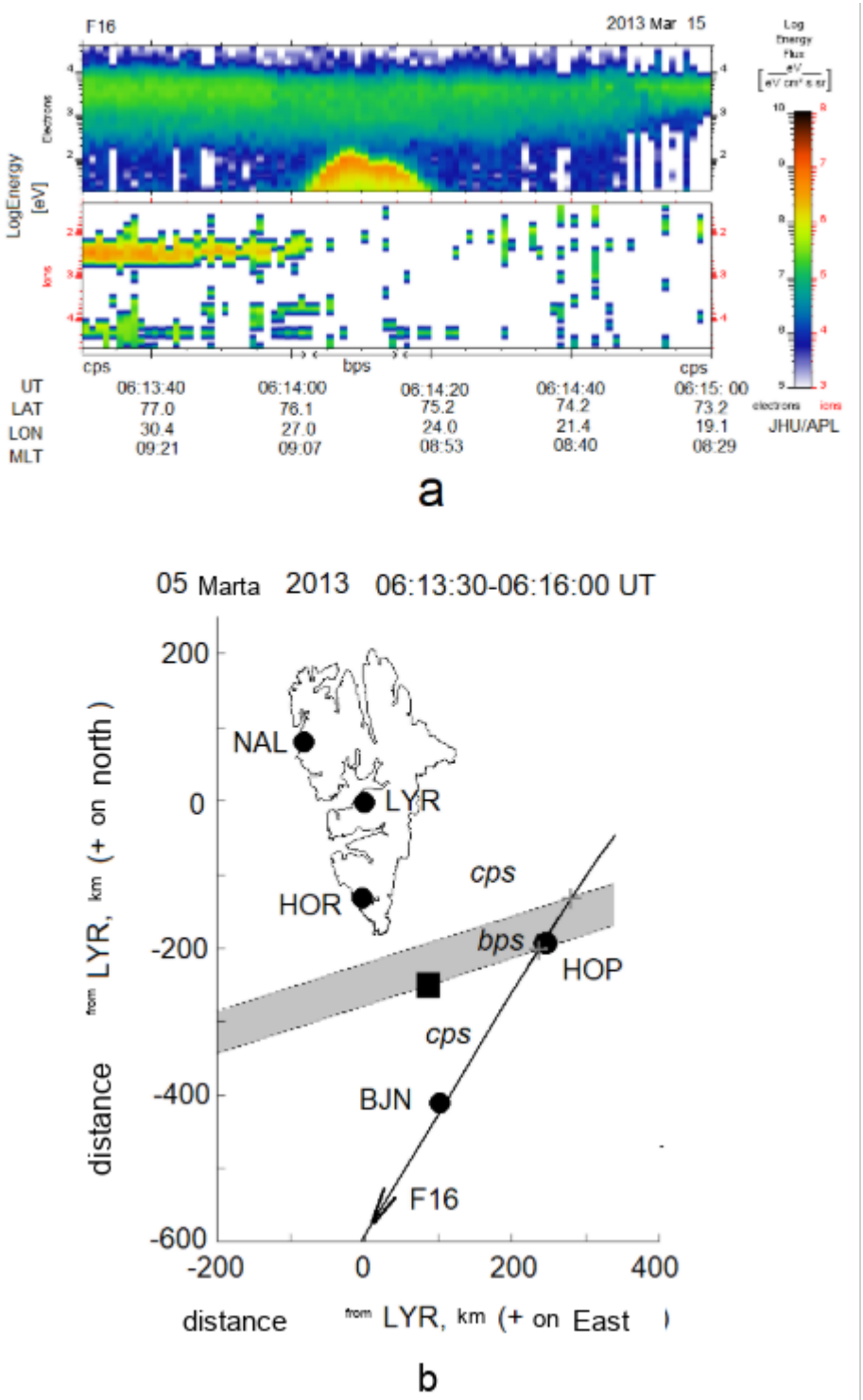
F16
2013 Mar 15
Log Energy Flux
LogEnergy [eV]
Electrons
Ions
cps
bps
cps
UT 06:13:40 06:14:00 06:14:20 06:14:40 06:15: 00
LAT 77.0 76.1 75.2 74.2 73.2
LON 30.4 27.0 24.0 21.4 19.1
MLT 09:21 09:07 08:53 08:40 08:29
JHU/APL
a
05 Marta 2013 06:13:30-06:16:00 UT
NAL
LYR
HOR
HOP
BJN
F16
cps
bps
cps
distance from LYR, km (+ on north )
distance from LYR, km (+ on East )
200
0
-200
-400
-600
-200
0
200
400
b

Fig. 2.

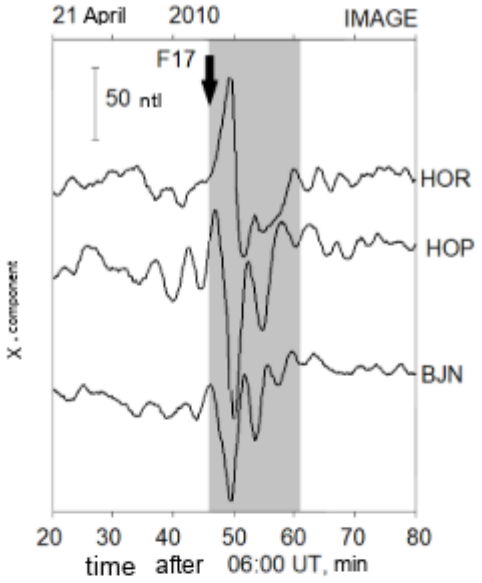
21 April 2010 IMAGE
F17
50 ntl
HOR
HOP
BJN
X - component
20 30 40 50 60 70 80
time after 06:00 UT, min

а

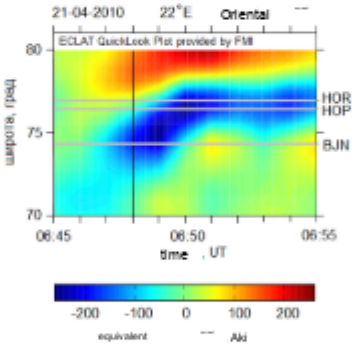
21-04-2010 22°E Oriental
ECLAT QuickLook Plot provided by FMI
80
75
70
HOR
HOP
BJN
06:45
06:50
06:55
time , UT
-200 -100 0 100 200
equivalent
Akl

b

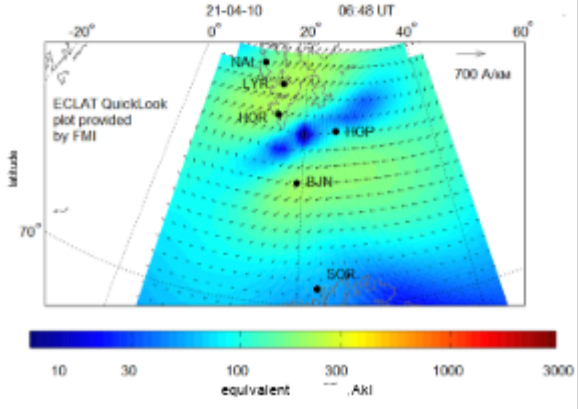
21-04-10 06:48 UT
-20° 0° 20° 40° 60°
NAL
LYR
HOR
HOP
BJN
SOR
700 A/км
ECLAT QuickLook
plot provided
by FMI
latitude
70°
10 30 100 300 1000 3000
equivalent
Akl

в

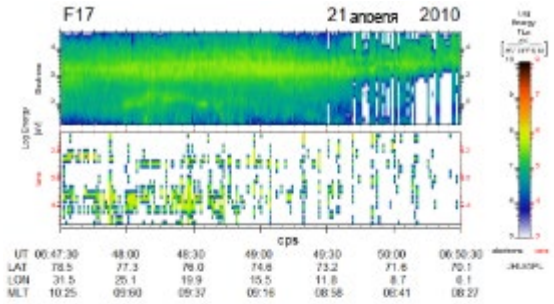
F17 21 апреля 2010
cps
UT 06:47:30 48:00 48:30 49:00 49:30 50:00 06:50:30
LAT 78.5 77.3 76.0 74.6 73.2 71.6 70.1
LON 31.5 25.1 19.9 15.5 11.8 8.7 6.1
MLT 10:25 09:50 09:37 09:16 08:58 08:41 08:27

г

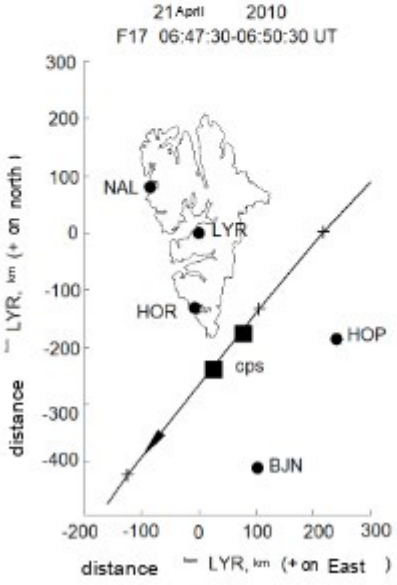
21 April 2010
F17 06:47:30-06:50:30 UT
300
200
100
0
-100
-200
-300
-400
NAL
LYR
HOR
HOP
cps
BJN
distance — LYR, km (+ on north )
-200 -100 0 100 200 300
distance — LYR, km (+ on East )

д

Fig. 3.

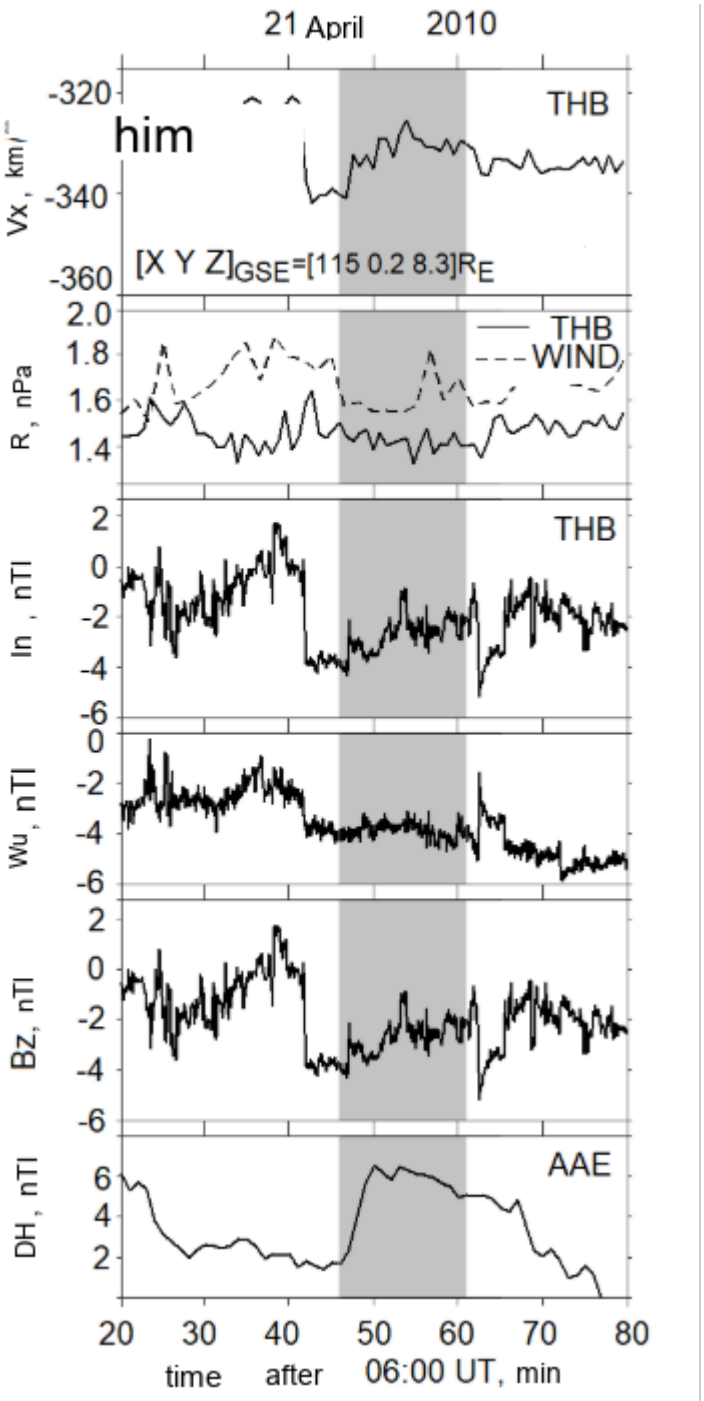
21 April 2010
him
THB
[X Y Z]GSE=[115 0.2 8.3]RE
Vx, km/s
-320
-340
-360
THB
WIND
R, nPa
2.0
1.8
1.6
1.4
THB
In , nTl
2
0
-2
-4
-6
Wu, nTl
0
-2
-4
-6
Bz, nTl
2
0
-2
-4
-6
AAE
DH, nTl
6
4
2
20
30
40
50
60
70
80
time after 06:00 UT, min

Fig. 4.

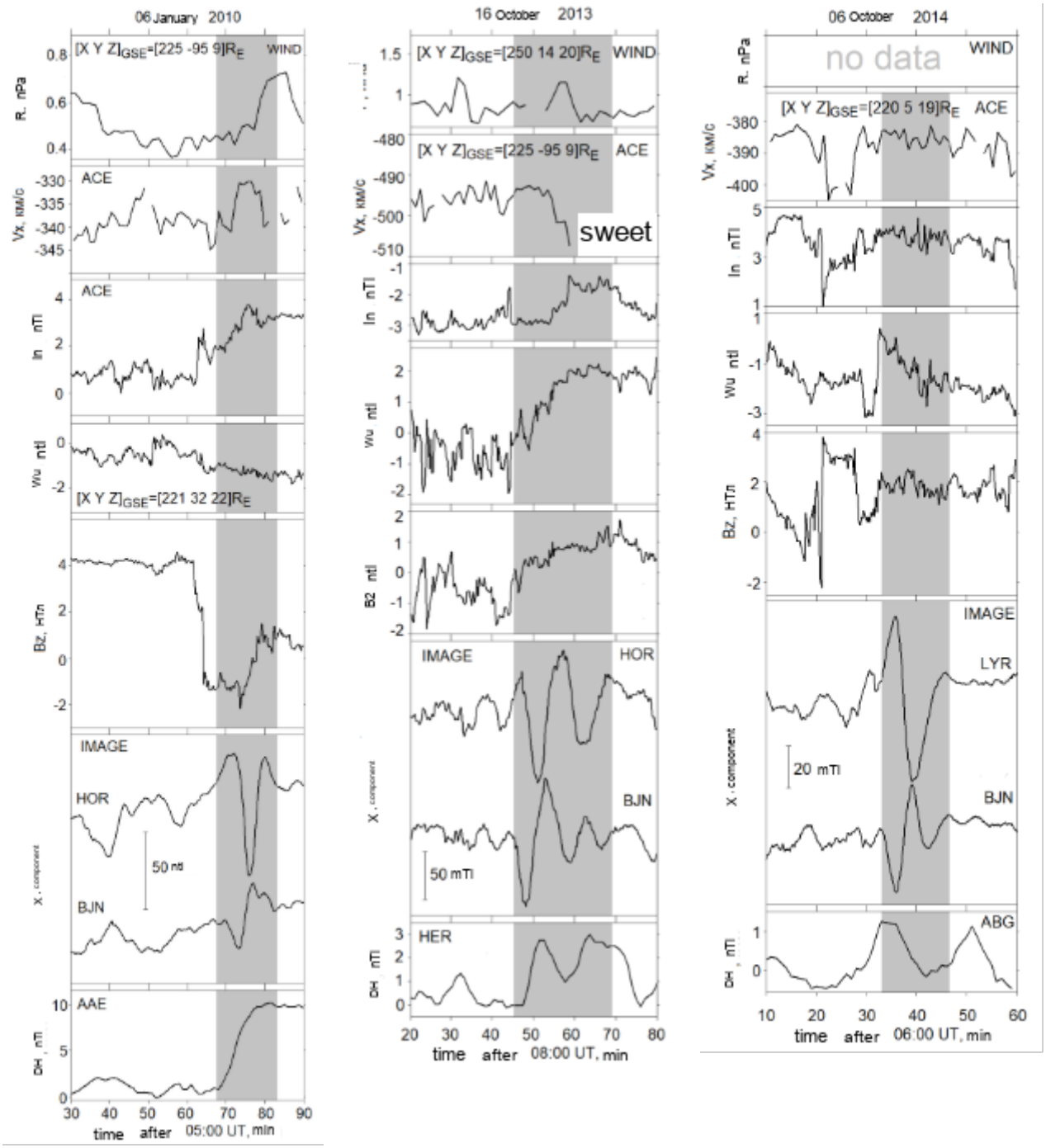
06 January 2010
[X Y Z]GSE=[225 -95 9]RE
WIND
R, nPa
ACE
Vx, KM/C
ACE
In nTl
Wu ntl
[X Y Z]GSE=[221 32 22]RE
Bz, HTn
IMAGE
HOR
50 ntl
BJN
X component
AAE
DH, nT
time after 05:00 UT, min
16 October 2013
[X Y Z]GSE=[250 14 20]RE
WIND
[X Y Z]GSE=[225 -95 9]RE
ACE
sweet
In nTl
Wu ntl
Bz ntl
IMAGE
HOR
50 mTl
BJN
X component
HER
DH nTl
time after 08:00 UT, min
06 October 2014
no data
WIND
[X Y Z]GSE=[220 5 19]RE
ACE
Vx, KM/C
In nTl
Wu ntl
Bz, HTn
IMAGE
LYR
20 mTl
BJN
X component
ABG
DH, nTl
time after 06:00 UT, min

*a* *b* *c*

Fig. 5.